A&A 542, A33 (2012)
DOI: 10.1051/0004-6361/201118101

Astronomy & Astrophysics

M-dwarf metallicities. A high-resolution spectroscopic study in the near infrared⋆,⋆⋆,⋆⋆⋆

A. Önehag[1], U. Heiter[1], B. Gustafsson[1], N. Piskunov[1], B. Plez[2], and A. Reiners[3]

[1] Department of Physics and Astronomy, Uppsala University, Box 516, S-751 20 Uppsala, Sweden
e-mail: Anna.Onehag@fysast.uu.se
[2] Laboratoire Univers et Particules de Montpellier, CNRS, Université Montpellier 2, 34095 Montpellier, France
[3] Universität Göttingen, Institut für Astrophysik, Friedrich-Hund-Platz 1, 37077 Göttingen, Germany

Recieved 15 September 2011 / Accepted 30 November 2011

ABSTRACT

Context. The relatively wide spread in the derived metallicities ([Fe/H]) of M dwarfs shows that various approaches have not yet converged to consistency. The presence of strong molecular features and incomplete line lists for the corresponding molecules have made determining the metallicity of M dwarfs difficult. Furthermore, the faint M dwarfs require long exposure times for the signal-to-noise ratio needed for a detailed spectroscopic abundance analysis.
Aims. We present a high-resolution ($R \sim 50\,000$) spectroscopic study of a sample of eight single M dwarfs and three wide-binary systems observed in the infrared J band.
Methods. The absence of large molecular contributions allows for a precise continuum placement. We derived metallicities based on the best fit of synthetic spectra to the observed spectra. To verify the accuracy of the applied atmospheric models and test our synthetic spectrum approach, three binary systems with a K-dwarf primary and an M-dwarf companion were observed and analysed along with the single M dwarfs.
Results. We obtain good agreement between the metallicities derived for the primaries and secondaries of our test binaries, thereby confirming the reliability of our method of analysing M dwarfs. Our metallicities agree well with some earlier determinations, and deviate from others.
Conclusions. We conclude that spectroscopic abundance analysis in the J band is a reliable method for establishing the metallicity scale for M dwarfs. We recommend its application to a larger sample covering lower, as well as higher, metallicities. Further prospects for the method include abundance determinations for individual elements.

Key words. stars: abundances – techniques: spectroscopic – stars: atmospheres – stars: low-mass – binaries: visual

1. Introduction

Although the M dwarfs constitute a large fraction of the detectable baryonic matter, we still lack a great deal of knowledge about our low-mass (<0.6 $M_\odot$) hydrogen-burning neighbours. Studies (Henry 1998; Chabrier 2003) suggest that as much as 70% of all stars in the solar vicinity (~10 pc) are M dwarfs, which makes these objects essential when deriving quantities such as the initial mass function (IMF, Salpeter 1955) and the present-day mass function. These frequently used functions are derived using the luminosity. The transformation to mass, based upon stellar evolution theories, is sensitive to chemical composition. Moreover, a study of the possible time dependence of the IMF function for the low-mass part needs good stellar metallicity criteria for M dwarfs. Thus, if we are to create a realistic model of the galactic evolution and current status, detailed studies of these faint but numerous objects are of great interest. The M dwarfs are needed for understanding main-sequence stellar evolution and defining a limit between stellar and substellar objects. Finally, a well defined metallicity scale for M dwarfs is essential to determine whether or not the general trend towards supersolar metallicities among FGK-stars planet hosts (e.g. Fischer & Valenti 2005) also holds for cooler objects.

Spectroscopic studies of M dwarfs at high resolution have proven to be a difficult task. In the low-temperature regime occupied by these stars ($2000 \lesssim T_{\rm eff} \lesssim 4100$ K), the optical spectrum is covered by a forest of molecular lines, hiding or blending most of the atomic lines used in spectral analysis. However, models of low-mass, late-type stars have undergone continuous improvements, from the early work by Tsuji (1969), Auman (1969), and Mould (1975, 1976) to the work by Brett & Plez (1993), Brett (1995a,b), Allard & Hauschildt (1995), Hauschildt et al. (1999) with their extensive grid of NextGen models, and the improved MARCS models (Gustafsson et al. 2008). New molecular and atomic line data are collected and organised in large databases such as VALD (Kupka et al. 1999) and VAMDC (Dubernet et al. 2010) and will improve the situation further.

The faintness characterising the M dwarfs has limited the number of high-resolution, high signal-to-noise studies. Insufficient resolution and dominant molecular features make it difficult to derive the accurate atomic line strengths needed for determining a reliable metallicity. Metallicities have been derived via photometric calibrations (Bonfils et al. 2005a), studies using molecular indices (Woolf & Wallerstein 2006), as well as spectrum synthesis (Bean et al. 2006a,b) and spectroscopic calibrations in the K band (Rojas-Ayala et al. 2010).

⋆ Based on data obtained at ESO-VLT, Paranal Observatory, Chile, Program ID 082.D-0838(A) and 084.D-1042(A).
⋆⋆ Table 2 is available in electronic form at http://www.aanda.org
⋆⋆⋆ Electronic version of the spectra is only available at CDS via anonymous ftp to cdsarc.u-strasbg.fr (130.79.128.5) or via http://cdsarc.u-strasbg.fr/viz-bin/qcat?J/A+A/542/A33

In this paper we present a detailed spectroscopic study in the J band (1100−1400 nm), which is a spectral region relatively free of molecular lines. In the near infrared, atomic lines can be isolated, and the lack of molecular lines allows a precise continuum placement. This spectral region was exploited for abundance analysis in the pioneering study of Betelgeuse, based on FTS spectra, by Vieira (1986), but has not been used much for late-type dwarfs until the last decade due to lack of efficient IR spectrometers at large telescopes. The present generation of IR echelles at large telescopes have, however, opened new possibilities, see, e.g. McLean et al. (2000, 2007).

As in previous studies (Bean et al. 2006b; Bonfils et al. 2005a), we select a number of binary systems with a solar-type primary and an M-dwarf companion to assess the accuracy of the atmospheric models used in the analysis and to verify the atomic line treatment. We then apply this result to a number of non-binary M dwarfs. Our choice of spectral region makes a careful analysis possible for a sample of stars that are thought to have a high metal content (−0.35 to 0.5 dex), avoiding the large contribution of molecules such as TiO to the spectrum at optical wavelengths.

The paper is organised as follows. In Sect. 2 we briefly summarise previous metallicity studies of M dwarfs. In Sect. 3, we describe the programme stars, the observations, and some aspects of the data reduction. In Sect. 4, the ingredients of the spectrum analysis are presented – compilation and derivation of spectral line data, stellar atmospheric parameters, and the procedure for metallicity estimation. In Sect. 5 we discuss the results of the analysis, and Sect. 6 concludes the paper.

2. Previous studies

The stars in our sample have been investigated with various other methods by several authors. In the following, we give a brief description of these studies.

Bonfils et al. (2005a) developed a photometric calibration of M-dwarf metallicities based on the spectroscopic analysis of FGK-type components of wide binary systems, where the secondaries are M dwarfs. They complemented their calibration sample with spectroscopic metallicities derived for metal-poor early-M-type dwarfs by Woolf & Wallerstein (2005). Based on these metallicities and 2MASS photometry for 46 stars, they derived an expression for the metallicity as a function of absolute K magnitude M_K and $V-K$ colour.

Bean et al. (2006a) analysed optical spectra with $R \geq 50\,000$ and signal-to-noise ratios between 200 and 400 of three stars. They used the methods developed in Bean et al. (2006b), fitting synthetic spectra for 16 atomic lines in the spectral intervals 8326 to 8427 and 8660 to 8693 Å, as well as a TiO bandhead at 7088 Å to their observations. They simultaneously determined $T_{\rm eff}$, metallicity, broadening parameters, and continuum normalisation factors from the spectra. Bean et al. (2006b) used five wide binary stars with FGK primaries and M-dwarf secondaries to evaluate their method (amongst them GJ 105). They found differences in derived metallicity between the M dwarf and solar-similar components ranging from −0.16 to −0.07 for four systems, and +0.03 dex for GJ 105.

Johnson & Apps (2009) and Schlaufman & Laughlin (2010) both aimed to improve the Bonfils et al. (2005a) photometric calibration, taking a slightly different approach. First, they used a volume-limited calibration sample of solar-type stars to derive the mean metallicity of the solar neighbourhood. Johnson & Apps (2009) selected 109 G0-K2 dwarfs with spectroscopically determined metallicities and distances $d < 18$ pc from Valenti & Fischer (2005). Schlaufman & Laughlin (2010) selected a sample of F and G dwarfs with metallicity estimates based on Strömgren photometry and $d < 20$ pc from Holmberg et al. (2009), which was kinematically matched to the solar-neighbourhood M-dwarf population.

Next, these authors defined a main-sequence line in the $(V-K)-M_K$ plane for a second calibration sample of late-K and M-type dwarfs. Johnson & Apps (2009) defined the second calibration sample of nearby low-mass stars to be a volume-limited sample of single K-type dwarfs ($d < 20$ pc) and single M-type dwarfs ($d < 10$ pc) based on parallaxes from Hipparcos and other sources. They fit a fifth-degree polynomial to the $V-K$ colours and M_K magnitudes of these stars. Schlaufman & Laughlin (2010) adopted the main-sequence line of Johnson & Apps (2009) for their study.

A third calibration sample was used to find the variation in metallicity with horizontal or vertical distances from the main-sequence line ($\Delta(V-K)$ or ΔM_K, respectively). Johnson & Apps (2009) used a set of six M dwarfs with FGK-companions with metallicities >+0.2 dex from Valenti & Fischer (2005) and assigned the mean metallicity of the first calibration sample to the main-sequence line. They derived a linear relationship between [Fe/H] and ΔM_K with a dispersion of 0.06 dex. Schlaufman & Laughlin (2010) extended this calibration set by adding 13 wide-binary stars with accurate V magnitudes from Bonfils et al. (2005a) with $-0.33 \leq$ [Fe/H] $\leq +0.32$. They derived a linear relationship between [Fe/H] and $\Delta(V-K)$, based only on the third calibration sample and the main-sequence line. In this case, the first calibration sample was used to verify that the zero point of this relationship is close to the mean metallicity of the solar neighbourhood.

The work of Rojas-Ayala et al. (2010) is based on low-resolution spectroscopy in the K band. They used a calibration sample of 17 M dwarfs in wide-binary systems with metallicities determined for the FGK primaries by Valenti & Fischer (2005). From these metallicities and their observations, they derived a linear relationship between [Fe/H], two metallicity-sensitive indices measured from Na I and Ca I features, and a temperature-sensitive water index. They estimate an uncertainty for their calibration of 0.15 dex.

3. Target selection and observations

We compiled a sample of M dwarfs in binary systems with a solar-type (FGK) primary companion and non-binary M dwarfs in the solar vicinity. Some of the M dwarfs or systems we observed are known to harbour planets, but others have no detection of any planet companions as yet. The programme stars were selected from the catalogue of nearby wide binary and multiple systems (Poveda et al. 1994) and from the Interactive Catalog of the on-line Extrasolar Planets Encyclopaedia (Schneider et al. 2011)[1], as well as from a programme searching for stellar companions of exoplanet host stars (Mugrauer et al. 2004, 2005, 2007).

The observations were carried out in service mode with the infrared spectrometer CRIRES at ESO-VLT (Kaeufl et al. 2004). In total 14 stars were observed during periods 82 (1 October 2008 to 31 March 2009) and 84 (1 October 2009 to 31 March 2010). A slit width of 0.4″ was used, resulting in a resolving power of $R = \lambda/\Delta\lambda = 50\,000$. In addition, a number of close binary systems with small separations ($\leq 20''$) were observed that will be discussed in a future paper. In this article we

[1] http://exoplanet.eu

Table 1. Selection of stars used in the analysis.

Target	Other ID	Type	Planet?	Period†	~S/N	Ref.	Ref. Planet
HD 101930A	HIP 57172	K2	yes	82	120	1	a
HD 101930B	TYC 8638-366-1	M0-M1		82	150	2	
GJ 105 A	HIP 12114	K3	no	82	110	1	
GJ 105 B	BD+06 398B	M4.5		84	80	3	
GJ 250 A	HIP 32984	K3	no	82	80	4	
GJ 250 B	HD 50281B	M2		82	100	5	
GJ 176	HIP 21932	M2	yes	82	70	5	b
GJ 317	LHS 2037	M3.5	yes	84	100	5	c
GJ 436	HIP 57087	M2.5	yes	84	140	5	d
GJ 581	HIP 74995	M3	yes	84	110	5	e
GJ 628	HIP 80824	M3.5	no	84	130	5	
GJ 674	HIP 85523	M2.5	yes	84	140	6	f
GJ 849	HIP 109388	M3.5	yes	82, 84	90, 120	3	g
GJ 876	HIP 113020	M4	yes	84	100	5	h

Notes. † ESO period in which our observations were taken.

References. For spectral types: 1) Gray et al. (2006); 2) Mugrauer et al. (2007); 3) Jenkins et al. (2009); 4) Upgren et al. (1972); 5) Reid et al. (1995); 6) Hawley et al. (1996). References for planet detections: a) Lovis et al. (2005); b) Endl et al. (2008); c) Johnson et al. (2007); d) Butler et al. (2004); e) Bonfils et al. (2005b); f) Bonfils et al. (2007); g) Butler et al. (2006); h) Marcy et al. (1998).

present the analysis of three wide binary systems and eight single M dwarfs. The binary systems are well separated and the angular separations are 73″ for HD 101930 (Mugrauer et al. 2007), 165″ for GJ 105 (van Maanen 1938), and 58.3″ for GJ 250 (Dommanget & Nys 2002). The observations of our stars should therefore not be contaminated with light from the companion star. GJ 105A has a faint, close-by (3″) low-mass companion, GJ 105C (Golimowski et al. 1995a,b). The luminosity difference in the J band however is of the order of five magnitudes and the fainter companion is assumed not to affect the analysis. See Table 1 for a list of spectral types, binarity, and planet detections of the stars treated in this paper. Each target was observed with four different CRIRES wavelength settings, centred on 1177, 1181, 1204, and 1258 nm in period 82, and 1177, 1205, 1258, and 1303 nm in period 84 (see Figs. 2 and 4 for the total wavelength coverage). For some of the fainter stars we obtained several exposures, which were co-added to reach a signal-to-noise ratio around 100. The typical continuum signal-to-noise ratio spans between 70 and 150.

CRIRES contains four detectors, but unfortunately only detectors #2 and #3 produced reliable data, since #1 and #4 are heavily vignetted and possibly contaminated by crosstalk between adjacent orders. Realising the extent of this failure of the first and fourth detectors, we chose to rearrange the wavelength settings between the observing periods. We re-observed one target from period 82 (GJ 849) in period 84 to assure consistency between the two observing runs. As is shown below (Sect. 5), our analysis indeed gives the same metallicity for both periods, which supports the homogeneity of our observations. The analysis in this paper is based on the higher reliability data from detectors #2 and #3.

In connection with each observation, a rapidly rotating early-type star, was observed to represent the telluric spectrum. Although the observed region (1167–1306 nm) was chosen to harbour as few telluric lines as possible, the majority of lines detected in the spectra still were of telluric origin. The pipe-line reduced spectra were normalised, together with the corresponding telluric standard to ensure a consistent continuum placement. The absence of strong molecular absorptions made continuum windows easily recognisable.

From a first examination of the reduced data it became clear that the wavelength calibration in ESO's reduction pipe-line based on thorium and argon lines did not produce the desired outcome. Both overall shifts and distortions in the wavelength scale could be seen, compared to the solar atlas or to synthetic spectra, probably because of the small number of thorium and argon lines present in the calibration frame of the observed wavelength regions. The solution was to make use of the telluric lines present in the observations and to match these with telluric lines in the electronic version of the atlas of the solar spectrum (Livingston & Wallace 1991)[2], using a polynomial fit.

4. Analysis

4.1. Spectral line data

The atomic line data in the observed region were acquired from the Vienna Atomic Line Database (VALD Kupka et al. 1999), with the exception of a few lines that are from Meléndez & Barbuy (1999). We used the Sun as a reference and calculated a synthetic spectrum using the established line list. A MARCS model with the parameters $T_{\rm eff} = 5777$ K, $\log g = 4.44$, [Fe/H] = 0.00 was adopted and $v \sin i = 1.7\,{\rm km\,s^{-1}}$ was used. We used the same solar chemical composition as in the MARCS models (Grevesse et al. 2007). The unknown line-broadening micro- ($\xi_{\rm t}$) and macroturbulence ($\zeta_{\rm t}$) parameters must be adjusted when comparing the synthetic spectrum with observed lines. We used a high-quality solar spectrum where telluric lines had been removed (Livingston & Wallace 1991) and the SME package (see Sect. 4.3) to solve for both turbulence parameters.

When comparing our solution with the observed spectrum we noted that a few lines did not match. This might be the result of inaccuracies in the listed oscillator strengths and damping parameters. We therefore determined new $\log gf$ and van der Waals broadening parameters for these particular lines (assuming that hydrogen is the main perturber in this temperature regime) . This was done in an iterative scheme where we first solved for the $\log gf$ and van der Waals parameters for each of the deviating lines separately, and then determined the turbulence parameters

[2] ftp://nsokp.nso.edu/pub/Kurucz_1984_atlas/photatl/

using all lines. After a few iterations we converged to a synthetic fit that reproduced the solar line profiles. The ξ_t and ζ_t values that yielded the best-fit were found to be 0.79 km s^{-1} and 1.77 km s^{-1}, respectively. The final line data for the dominant lines used in the metallicity analysis can be found in Table 2, where we have marked the lines for which we redetermined the line parameters.

The observed wavelength region was chosen to contain as few stellar molecular features as possible. Significant stellar molecular absorption in the observed wavelength regions comes from FeH. In addition, some absorption from CrH and water is expected.

Spectral lines of FeH were synthesised for all targets together with the atomic lines, to account for possible blends. The FeH line list was calculated by one of us (BP), using the best available laboratory data for energy levels and transition moment (Phillips et al. 1987; Langhoff & Bauschlicher 1990). The weak FeH lines visible in the spectra of our M dwarfs seem to be reproduced rather well. We compared our FeH line list with that of Dulick et al. (2003) by calculating spectra with both lists for the two stars GJ 436 and GJ 628. An overall comparison showed that the FeH lines calculated with the Dulick et al. (2003) list were somewhat weaker than when using the BP list. Line-depth ratios between a number of selected FeH lines appearing in both lists and in the observations were calculated. For this calculation, we used mean fluxes of the 40% of the pixels closest in wavelength to the line centre within the regions masking each FeH line, such as those shown in Fig. 1. The BP ratios were closer to the observed ones than the Dulick ratios for a majority of these lines – for GJ 436 for 20 out of 30 lines, and for GJ 628 for 22 out of 37 lines. The spectra calculated with the Dulick et al. (2003) list contain several lines that do not appear in the BP list and which we do not observe in our spectra. In conclusion, we decided to use the BP list for the analysis. After the completion of the present paper we noted that the line list by Dulick et al. (2003) has been used by Wende et al. (2010) to model CRIRES spectra of a late M dwarf in the wavelength range 986–1077 nm and subsequently by Shulyak et al. (2011) for a study of rotation and magnetic fields in late-type M-dwarf binaries.

We also synthesised the observed spectral regions including CrH lines with data taken from Burrows et al. (2002) for a representative set of parameters. The regions contain a few weak CrH lines, but they do not coincide with any of the atomic lines selected for analysis, and thus were not taken into account.

We assessed the importance of water absorption for our spectral region by computing synthetic spectra using the line list of Barber et al. (2006). From the ≈27 million theoretical transitions listed between 1160 and 1320 nm, we removed those with a line strength of less than 0.5% of the strongest line at $T = 3000$ K (the line strength measure was $\log(\lambda)+\log(gf)-E_{\rm low}/(\ln 10kT)$), resulting in 57 265 lines. We computed pure water spectra for atmospheric models with a range in $T_{\rm eff}$ and metallicity corresponding to our M-dwarf sample. If the line parameters are correct, spectra with $T_{\rm eff} = 3200$ K may suffer from a decrease in the continuum level of up to 2%, caused by numerous weak water lines. For higher temperatures, the importance of water absorption decreases rapidly. For wavelengths less than about 1200 nm, individual water lines with depths of up to 5% are apparent in the test calculations for $T_{\rm eff} = 3200$ K. We also calculated spectra for the parameters of GJ 628 (see Sect. 4.2) for the four wavelength segments with $\lambda < 1208$ nm, including atomic, FeH, and water lines, and compared them with the observations. There was a weak resemblance between some of the synthetic water lines and some of the otherwise unidentified features in the observed spectra, but we could not verify the accuracy of the wavelengths and line strengths to a satisfactory degree. Also, the profiles of the atomic lines showed little change in the spectra with and without water absorption. We therefore decided not to include the water line list in the analysis.

4.2. Atmospheric parameters

The analysis using synthetic spectra requires a specification of several input parameters: effective temperature, $T_{\rm eff}$, surface gravity, $\log g$, the macro- and microturbulence parameters, and the overall metallicity [Fe/H] compared to the Sun. We searched the archives (e.g. SIMBAD, VizieR) to find reliable measures of the atmospheric parameters. We found spectroscopically determined values for the three K-dwarf stars in our sample and used an unweighted mean based on these values. The adopted atmospheric parameters can be found in Table 3. For the majority of the M-dwarf targets there are no detailed atmospheric studies available. To keep the analysis consistent, effective temperatures and surface gravities for the M-dwarf targets were determined using calibration equations based on photometric data. High-accuracy photometric data were available in the archives for all of our stars. Photometric data in the Johnson (BV) and Cousins $(RI)_{\rm c}$ systems were collected, and an unweighted mean was calculated where multiple measures were available. Infrared colours (JHK) were gathered from the Two Micron All Sky Survey (2MASS: Cutri et al. 2003), see Table 4.

Effective temperatures for the M dwarfs were estimated from the photometric calibrations derived by Casagrande et al. (2008), using different combinations of the V, $R_{\rm c}$, $I_{\rm c}$, J, H, $K_{\rm s}$ colours. The resulting twelve $T_{\rm eff}$ values per target were then merged into a mean. We noted that our main molecular features, the FeH lines, are quite temperature sensitive. We used this sensitivity to verify and adjust the photometric temperatures. The FeH lines show good agreement for most photometric temperatures, whereas they indicate a correction by up to +200 K for a few objects (see Table 5). We estimated the uncertainties of the photometric temperatures by propagating the uncertainties of the observed colours through the calibrations. To this we added the quoted uncertainty of the calibration expression itself in quadrature. The resulting uncertainties of ∼150 K for the photometric temperatures is in good agreement with the corrections we apply based on the temperature sensitivity of FeH. An example is shown in Fig. 1, where a synthetic spectrum with three different $T_{\rm eff}$ values is compared to a region of the observed spectrum of GJ 436 containing several FeH lines. The $T_{\rm eff}$ values correspond to the photometric $T_{\rm eff}$, as well as 200 K lower and higher values. We adjusted the temperature and metallicity for four of the M dwarfs iteratively, since the FeH line strengths also depend on the overall metallicity. We tested the sensitivity of the FeH lines to surface gravity and did not find any significant effect in the parameter space and wavelength regions relevant to this study, unlike Wende et al. (2009), who find a surface gravity sensitivity using 3D-models. That study, however, was carried out in a different wavelength region (997 nm) and with a larger stepsize in $\log g$ than tested for here.

In addition, the tabulated grids of colours by Worthey & Lee (2011) were used to estimate a value for the effective temperature, gravity, and metallicity simultaneously from an independent calibration. The best-fit set of parameters was determined via a chi-square minimisation between observed and tabulated colours ($B-V, J-K, H-K, V-K, V-I, V-R$). This method resulted in $T_{\rm eff}$ values similar to the adjusted Casagrande et al. (2008) calibrations (any differences are below 100 K). In Table 5 we list effective temperatures derived from both methods. We

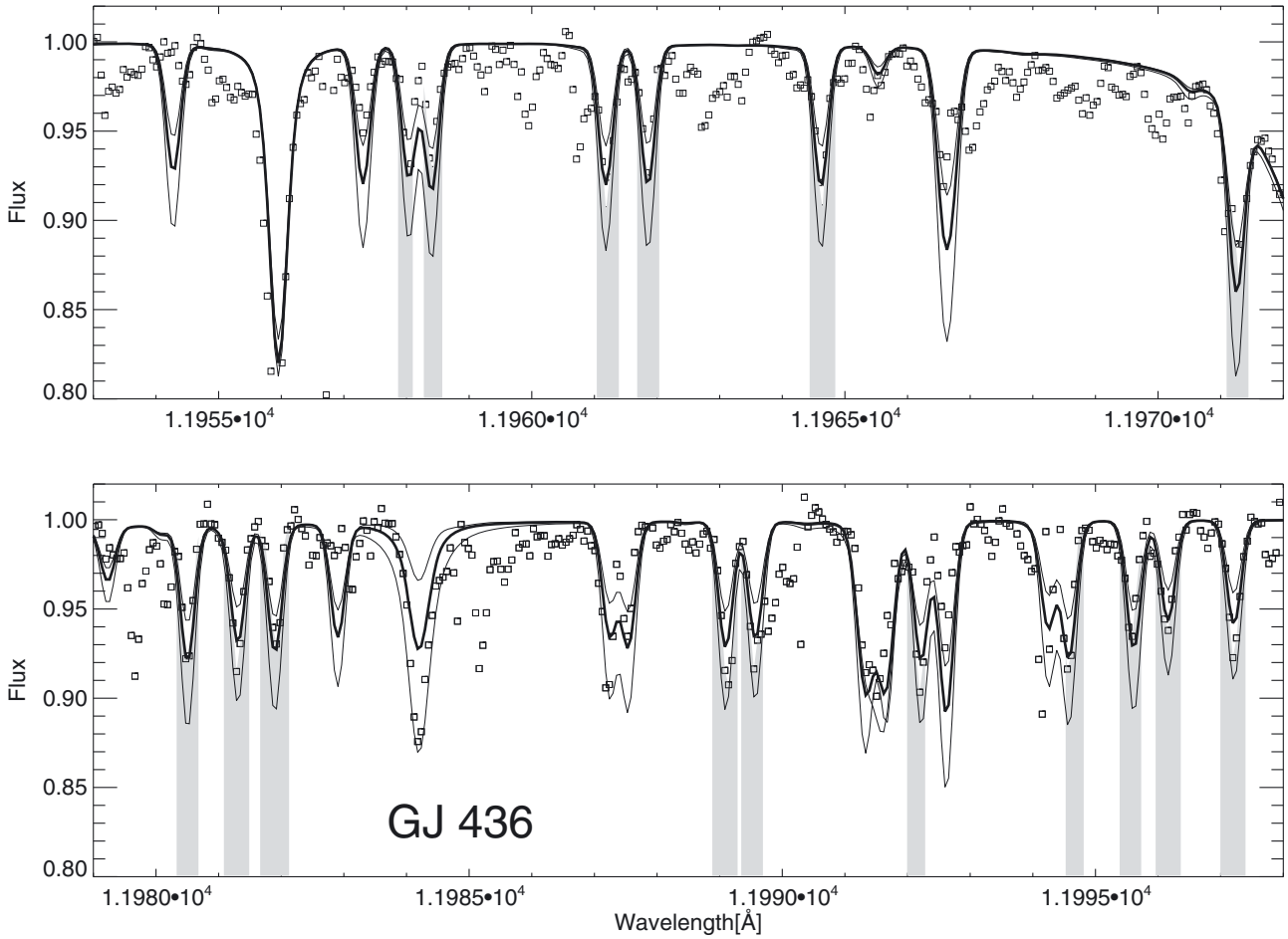

Fig. 1. Two selected wavelength regions containing FeH lines, with synthetic and observed spectra for GJ 436. The FeH lines are marked in grey shading. The thick solid line was calculated using the adopted $T_{\rm eff}$ of 3263 K. The upper and lower thin lines are calculated with 200 K higher and lower $T_{\rm eff}$ values, respectively. The observations are represented by open squares.

Table 3. Atmospheric parameters for the K stars.

Target	$T_{\rm eff}$ [K]	$\log g$ [cm s^{-2}]	$\xi_{\rm t}$ [km s^{-1}]	$v \sin i$ [km s^{-1}]	References
HD 101930 A	5121 ± 87	4.32 ± 0.19	0.82 ± 0.14	0.7	1, 2, 9
GJ 105 A	4867 ± 114	4.60 ± 0.07	0.60 ± 0.32	2.9	5, 6, 7, 8, 5
GJ 250 A	4758 ± 173	4.40 ± 0.33	0.64 ± 0.56	1.8	3, 4, 5, 6, 7, 5

References. 1) Sousa et al. (2008); 2) Santos et al. (2005); 3) Santos et al. (2004); 4) Mishenina et al. (2004); 5) Valenti & Fischer (2005); 6) Luck & Heiter (2006); 7) Heiter & Luck (2003); 8) Bean et al. (2006b); 9) Lovis et al. (2005). The $v \sin i$ reference is stated to the right in the list of references. The miroturbulent velocity for GJ105A is from references 6, 7, 8, and from references 3, 6, 7 for GJ250A.

take the maximum difference between the two $T_{\rm eff}$ determinations as an indication of the range of $T_{\rm eff}$ values to explore in the analysis for each target.

The surface gravities of the M dwarfs were established using the $\log g$–$\mathcal{M}_\star$ relation derived by Bean et al. (2006b, their Eq. (2)). The input masses were estimated from the $\log(\mathcal{M}/\mathcal{M}_\odot) - M_K$ relationship established by Delfosse et al. (2000). The M_K in this relation refers to the absolute K magnitude in the CIT system and a transformation of the 2MASS $K_{\rm S}$ magnitudes was carried out using the equation presented in Carpenter (2001). Absolute magnitudes in $K_{\rm CIT}$ were derived using the Hipparcos parallaxes (van Leeuwen 2007) for all targets except for GJ 317 and GJ 105 B where the parallaxes were taken from Johnson et al. (2007) and Jenkins et al. (2009), respectively. An estimate of the total $\log g$ error was made by propagating the uncertainties in the 2MASS $K_{\rm S}$ colours and listed parallax uncertainties through the calibration equations. In the absence of an error estimate of the mass-luminosity relation we derived the standard deviation of the mass-luminosity fit using the data on which the calibration expression is based (Delfosse et al. 2000, their Table 3). The surface gravity-mass calibration is determined by Bean et al. (2006b) to have an error of 0.08 [$\log$(cm s^{-2})] in $\log g$. Ignoring possible errors in the $K_{\rm S}$–$K_{\rm CIT}$ transformation, the different uncertainties were added in quadrature to calculate the final overall error (see Table 5).

4.3. Model atmospheres and abundance determination

For the metallicity determination we employed the method of fitting synthetic spectra to the observed spectra. The analysis is

Table 4. Stellar colours in the Johnson-Cousins and 2MASS systems.

Target	B	V	R_C	I_C	J	H	K_S	Reference
HD 101930 A	9.12	8.21			6.645 ± 0.019	6.259 ± 0.047	6.147 ± 0.026	2
HD 101930 B	11.663	10.605			7.940 ± 0.025	7.291 ± 0.049	7.107 ± 0.024	4
GJ 250 A	7.64	6.59	5.975	5.45	5.013 ± 0.252	4.294 ± 0.258	4.107 ± 0.036	1, 3
GJ 250 B	11.57	10.08	9.04	7.80	6.579 ± 0.034	5.976 ± 0.055	5.723 ± 0.036	9
GJ 105 A	6.78	5.81	5.235	4.74	4.152 ± 0.264	3.657 ± 0.244	3.481 ± 0.208	1, 3
GJ 105 B	13.16	11.66	10.44	8.88	7.333 ± 0.018	6.793 ± 0.038	6.574 ± 0.020	9
GJ 176	11.50	9.966	8.941	7.711	6.462 ± 0.024	5.824 ± 0.033	5.607 ± 0.034	8, 10
GJ 317	13.488	11.985	10.862	9.375	7.934 ± 0.027	7.321 ± 0.071	7.028 ± 0.020	1, 9
GJ 436	12.17	10.65	9.58	8.24	6.900 ± 0.024	6.319 ± 0.022	6.073 ± 0.016	10
GJ 581	12.179	10.571	9.456	8.051	6.706 ± 0.025	6.095 ± 0.033	5.837 ± 0.022	1, 9, 7, 8, 11
GJ 628	11.657	10.082	8.918	7.410	5.950 ± 0.024	5.373 ± 0.040	5.075 ± 0.024	1, 9, 7, 5, 6
GJ 674	10.944	9.389	8.312	6.979	5.711 ± 0.019	5.154 ± 0.033	4.855 ± 0.018	1, 9, 8, 11
GJ 849	11.878	10.376	9.284	7.877	6.510 ± 0.024	5.899 ± 0.044	5.594 ± 0.017	1, 9, 7, 8, 11
GJ 876	11.759	10.187	9.006	7.446	5.934 ± 0.019	5.349 ± 0.049	5.010 ± 0.021	1, 7, 5, 6, 11

Notes. All J, H, and K_S values are from 2MASS (Cutri et al. 2003).

References. For B, V, R_C, and I_C: 1) Bessel (1990); 2) Cousins & Stoy (1962); 3) Cousins (1980); 4) Kharchenko (2001); 5) Kilkenny et al. (1998); 6) Kilkenny et al. (2007); 7) Koen et al. (2002); 8) Koen et al. (2010); 9) Laing (1989); 10) Reid et al. (2004); 11) The et al. (1984).

Table 5. Atmospheric parameters for the M dwarfs.

Target	$T_{\rm eff}$ [K]	$T_{\rm eff}$ [K] (WL11)	$\log g$ [cms^{-2}]	Mass [$M_\odot$]	Parallax [mas]	$v \sin i$ [km s^{-1}]	Ref.
HD 101930 B	3908	3887	4.46 ± 0.09	0.70 ± 0.02	34.24 ± 0.81		
GJ 105 B	3261††	3162	4.96 ± 0.08	0.26 ± 0.01	129.4 ± 4.3	≤2.4	1
GJ 250 B	3376	3462	4.80 ± 0.08	0.44 ± 0.01	114.81 ± 0.44	≤ 2.5	1
GJ 176	3361	3462	4.76 ± 0.08	0.49 ± 0.02	107.83 ± 2.85		
GJ 317	3325††	3199	4.97 ± 0.12	0.25 ± 0.06	109 ± 20	≤2.5	1
GJ 436	3263	3376	4.80 ± 0.08	0.44 ± 0.01	98.61 ± 2.33	1.0 ±0.9	2
GJ 581	3308†	3288	4.92 ± 0.08	0.30 ± 0.01	160.91 ± 2.61	0.4 ±0.3	2
GJ 628	3208†	3167	4.93 ± 0.08	0.29 ± 0.01	232.98 ± 1.60	1.5	3
GJ 674	3305	3376	4.88 ± 0.08	0.35 ± 0.01	220.24 ± 1.42	3.2 ± 1.2	4
GJ 849	3196	3258	4.76 ± 0.08	0.49 ± 0.01	109.94 ± 2.07	≤2.4	5
GJ 876	3156†	3167	4.89 ± 0.08	0.33 ± 0.01	213.28 ± 2.12	≤2.0	5

Notes. Column descriptions: $T_{\rm eff}$ [K]: adopted effective temperatures, based on the Casagrande et al. (2008) calibration and FeH spectrum adjustment. † and †† denotes an increase in the photometric temperature by +100 and +200 K, respectively. $T_{\rm eff}$ [K] (WL11): effective temperatures derived from the Worthey & Lee (2011) calibration. Parallaxes are from Hipparcos (van Leeuwen 2007) for all targets except for GJ 317 (Johnson et al. 2007) and GJ105 B (Jenkins et al. 2009).

References. For $v \sin i$: 1) Browning et al. (2010); 2) Marcy & Chen (1992); 3) Reiners (2007); 4) Torres et al. (2006); 5) Delfosse et al. (1998).

based on the latest generation of MARCS model atmospheres (Gustafsson et al. 2008). These models give the temperature and pressure distribution in radiative and hydrostatic equilibrium, assuming radiative transport with mixing-length convection in a plane-parallel stellar atmosphere. The formation of dust is not accounted for in the models, as it has been found to be less important in models of early-type M dwarfs (earlier than about M6 or $T_{\rm eff} \gtrsim 2600$ K; Jones & Tsuji 1997; Tsuji 2002). Our sample includes rather early-type M dwarfs, see Table 1.

We used an improved version of the SME package (Valenti & Piskunov 1996; Valenti & Fischer 2005). This tool performs an automatic parameter optimisation using a Levenberg-Marquardt chi-square minimisation algorithm. Synthetic spectra are calculated on the fly by a built-in spectrum synthesis code, for a set of global model parameters and specified spectral line data. Starting from user-provided initial values, synthetic spectra are computed for small offsets in different directions for a subset of parameters defined to be "free". The required model atmospheres are interpolated in the grid of MARCS models available on the MARCS webpage[3], using an accurate algorithm described in Valenti & Fischer (2005, Sect. 4.1). Partial derivatives calculated from the corresponding parameter and chi-square values are used to approach the minimum on the chi-square surface. In an independent step from the parameter optimisation, the wavelength scale is corrected for any residual velocity shifts by a one-dimensional golden section search. SME also has the option to apply a local fit of the continuum, but we did not use this functionality here. Continuum normalisation was instead done during data reduction (see Sect. 3).

A mask specifies the pixels in the observed spectrum that should be used to determine velocity corrections and to calculate the chi-square. Mask definition is an important step in spectrum synthesis analysis. The radial velocity correction was done in a first step, using most of the observed spectral region and solar metallicity synthetic spectra. This correction was applied to the observed spectra before defining the mask for the metallicity analysis. We placed the mask as consistently as possible for all programme stars to cover the maximum number of spectral lines not affected by blends between different species. Defects in the observed spectra caused by imperfect telluric correction or instrumental effects were masked out, as were the cores of

[3] http://marcs.astro.uu.se

strong lines. For some blended or contaminated lines, a part of the profile was included in the mask if considered useful for the fitting procedure.

The number of available lines in the telluric-free spectra used in the analysis was at maximum 30 in a K dwarf and 23 in an M-dwarf spectrum. The total number of lines included in the analysis of each target spectrum varied slightly owing to differences in the data quality, imperfect telluric line removal and other non-physical spectral features. We encountered a problem with the four potassium lines in our spectra (1169.02, 1176.96, 1177.28, 1252.21 nm). When the gf-values were adjusted to fit a high-quality solar spectrum, the K lines became too strong in the cooler, high-gravity M dwarfs. We concluded that the lines are most likely affected by non-LTE in the solar spectrum. A discussion of the solar non-LTE effect of these lines can be found in Zhang et al. (2006), where two of the K lines present in our spectra are explored. These authors derive a negative abundance correction for the K lines, meaning that the lines are stronger when calculated in non-LTE than for LTE. Due to the higher densities, collisions may be expected to drive the atmospheres of M dwarfs towards LTE conditions. Although the non-LTE effects in the M dwarfs are probably less than in the Sun, they are as yet unknown to us. Hence, we decided not to use the K lines in the analysis and excluded them from our line mask (see Figs. 2 and 3).

There are nine C I lines apparent in the spectra of the Sun and the K dwarfs in our wavelength range. We tried to model these lines using atomic data from Ralchenko et al. (2010), which are based on averaged calculated transition probabilities from two literature sources (Nussbaumer & Storey 1984; Hibbert et al. 1993, using the "velocity" results of the latter), and van der Waals broadening parameters from Barklem et al. (2000). However, the synthetic lines were too weak in the solar spectrum and at the same time somewhat too strong in the K-dwarf spectra, compared to the observations. We were therefore not able to derive "astrophysical" gf-values applicable to both types of stars. We suspect non-LTE effects to be the cause of this problem, which might be spectral-type dependent, in the sense that they are stronger in G-type dwarfs than in K-type dwarfs. This is supported by the fact that all of these lines are high-excitation lines, with lower level energies lying between 7.5 and 8.8 eV. Such levels are easily depopulated by photoionization, which leads to deviations from the LTE approximation. We are not aware of any study of non-LTE effects for the carbon lines in question and therefore we did not include the carbon lines in the analysis.

For all other elements included in our investigation, we do not suspect any non-LTE effects based on the comparisons with the solar spectrum and the K-dwarf spectra. However, we cannot completely exclude any additional non-LTE effects based on our data and models. Unfortunately, non-LTE studies in the infrared region are rare, and investigations have focused on solar-type stars. The study by Allende Prieto et al. (2004) indicates that lines of neutral Fe and Ca might be affected by departures from LTE in the coolest stars of their sample. However, the lowest $T_{\rm eff}$ that they explore is close to 4500 K, and their spectral range extends from about 360 nm to 1 micron. For a review of non-LTE effects in optical spectra of FGK-type stars for a large number of elements, see Asplund (2005).

The consistency of the SME solution with the selected surface gravity could be tested using strong lines with well developed wings. While we are not sure about non-LTE effects on potassium line strength, we can try to use the shape of these lines for a gravity test. To do that we solved for the surface gravity keeping all the other parameters fixed from the optimal solution. The experiment was carried out for one data set for two objects, GJ 105B and GJ 628. We find that the surface gravities did not change by more than 0.03 dex, confirming that the preset values are consistent with the shapes of strong lines.

We let the overall metallicity, [Fe/H], and the macroturbulence parameter vary and solved for both simultaneously. For the M dwarfs, the unknown microturbulence parameter was set to 1 km s^{-1} and line broadening by rotation was neglected, as most of our M dwarfs are known to be relatively slow rotators (see Table 5). Since macroturbulence was the only line-broadening parameter, which we included in the fit procedure, the value resulting in the best-fit contains contributions from other broadening mechanisms, otherwise unaccounted for, e.g. variations in the instrumental profile, or rotational broadening. The derived values for our programme stars are below 1 km s^{-1}, except for GJ 876 (1.7 km s^{-1}), GJ 250A and B ($\approx$2 km s^{-1}), GJ 674 (3.8 km s^{-1} comparable to its $v \sin i$ value in Table 5), and GJ 105B (4.6 km s^{-1}).

To ensure that we end up in a global minimum when converging to a solution for the best-fit, we started from different initial values for the metallicity and plotted the resultant χ^2 for each fit as a function of the determined metallicity. This also gave us an estimate of the uncertainties introduced by the fitting routine itself, and was included in the total error calculation. A majority of the lines included in the analysis are weak, although some stronger lines are present. We tested the convergence dependence on weak lines as compared to the wings of the stronger lines and found that the strong and weak lines contributed equally to the final χ^2 solution. Both strong and weak lines resulted in equal metallicities. We also estimated the Ca abundances for the M dwarfs observed in period 84, where a number of Ca lines are present in the wavelength setup, and find [Ca/Fe] abundances of 0.0–0.1 dex with respect to solar values.

The total uncertainties were computed by perturbing the atmospheric parameters by $\pm$100 K in $T_{\rm eff}$ and $\pm$0.1 dex in $\log g$, and repeating the metallicity fit. The deviations with respect to the adopted [Fe/H] value were then added in quadrature to the uncertainties from the fitting routine itself.

5. Results and discussion

We have carried out a careful analysis of high-resolution M and K dwarf spectra in the infrared J band. To calibrate our metallicity scale, three binary systems consisting of a K-dwarf primary and an M-dwarf secondary were observed. The derived metallicities of the binary systems, as well as the single M dwarfs can be found in Table 6 and Fig. 5. In this table and figure we also list metallicities determined by previous spectroscopic and photometric investigations.

5.1. Binary systems

Stars in binary systems have been formed out of the same molecular cloud and are expected to have the same metallicities. For two of the three binary systems present in this study, we derive very similar metallicities for both components.

The binary system GJ250 AB consists of a K3-dwarf primary and an M2-dwarf secondary. The metallicity determinations for the two stars are consistent within the errors. The synthetic spectra calculated for both stars show good agreement for both weaker and stronger lines, including the potassium lines in the M dwarfs that are not included in the derivation of the best-fit (see Figs. 2 and 3).

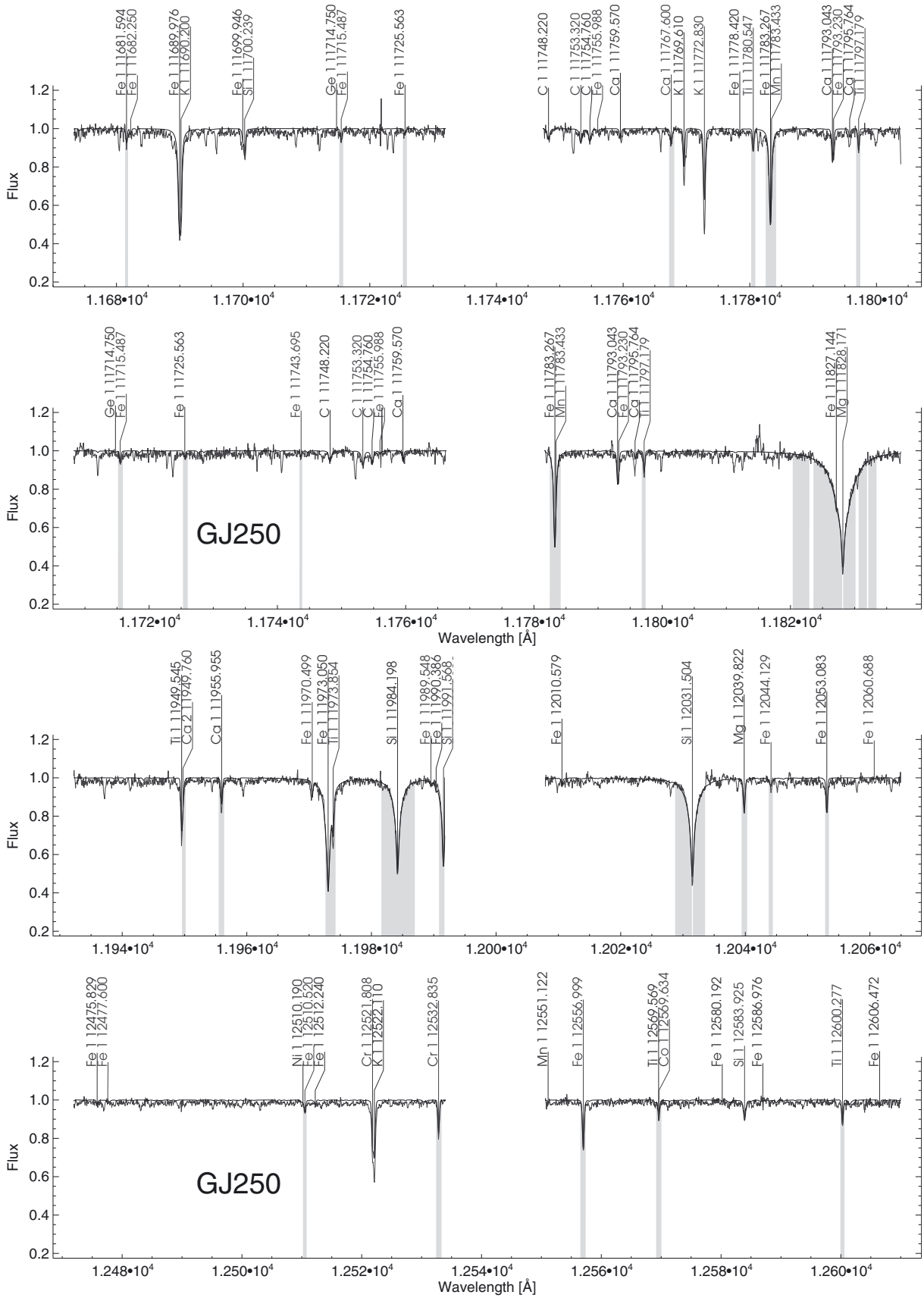

Fig. 2. The eight observed wavelength regions in period 82 plotted with the best-fit synthetic spectrum for GJ250A (primary in double system). The mask used in the metallicity determination is marked in grey shading.

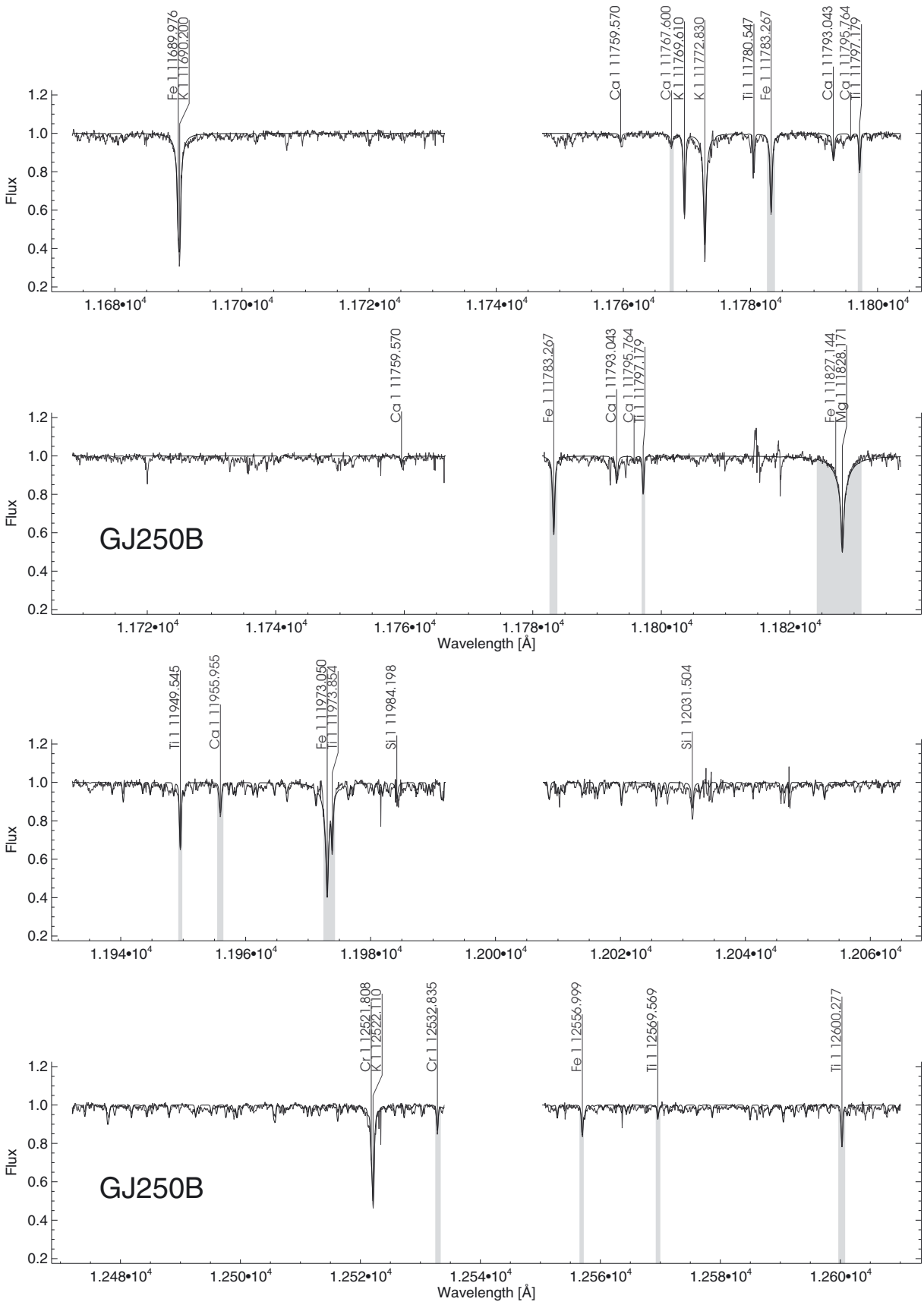

Fig. 3. The eight observed wavelength regions in period 82 plotted with the best-fit synthetic spectrum for GJ250B (secondary in double system). The mask used in the metallicity determination is marked in grey shading.

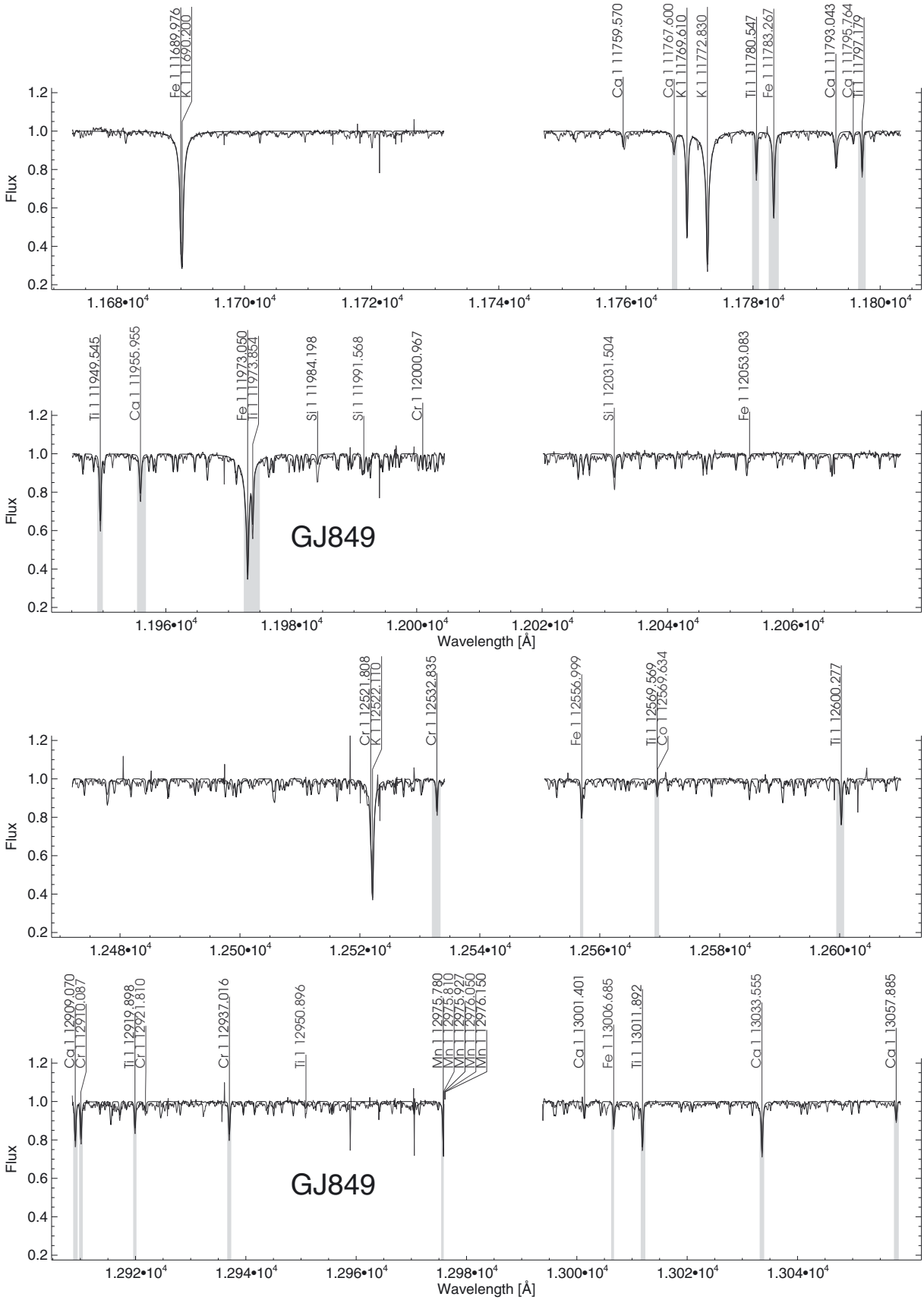

Fig. 4. The eight observed wavelength regions plotted with the best-fit synthetic spectrum for one of the coolest stars, GJ849 observed in period 84. The mask used in the metallicity determination is marked in grey shading.

Table 6. Derived metallicities for our sample and comparison with previous abundance determinations.

Target	This work	Bo05	Be06	JA09	SL10	R10
HD 101930A	+0.20 ± 0.06					
HD 101930B	+0.09 ± 0.10	−0.16		+0.08 c	−0.05	
GJ105A	−0.05 ± 0.01	−0.19 s	−0.12			
GJ105B	−0.06 ± 0.15	−0.15	−0.09	+0.06 c	−0.07	
GJ250A	−0.03 ± 0.05	−0.15 s				
GJ250B	−0.05 ± 0.05	−0.18		+0.05 c	−0.09	−0.04
GJ176	+0.04 ± 0.02	−0.06		+0.18	+0.05	
GJ317	+0.20 ± 0.14	−0.22		−0.10 c	−0.21	
GJ436	+0.08 ± 0.05	−0.05	−0.32	+0.25	+0.08	+0.00
GJ581	−0.15 ± 0.03	−0.25	−0.33	−0.10	−0.21	−0.02
GJ628	+0.08 ± 0.03	−0.13		+0.12 c	−0.02	
GJ674	−0.11 ± 0.13	−0.28		−0.11	−0.22	
GJ849 P82&84	+0.35 ± 0.10	+0.17		+0.58	+0.37	+0.49
GJ876	+0.12 ± 0.15	+0.02	−0.12	+0.37	+0.24	+0.43

Notes. Column descriptions: this work: our results. The quoted errors are a combination of systematic errors from the uncertainties in atmospheric parameters and the uncertainty from the fitting routine (see Sect. 4.3). Bo05: values calculated from the calibration equation of Bonfils et al. (2005a), except for those marked with an "s", which are spectroscopically determined. Be06: Bean et al. (2006a). JA09: values from Johnson & Apps (2009), except for those marked with a "c", which are determined from our collected colours and the provided calibration (extrapolation slightly outside the valid range for HD 101930B). SL10: values calculated from the calibration equation of Schlaufman & Laughlin (2010). R10: Rojas-Ayala et al. (2010).

The M dwarf in the GJ105 AB system shows FeH lines that are too weak in comparison to the calculated spectrum based on the derived photometric effective temperature. We adjusted the temperature by +200 K while solving for [Fe/H] simultaneously as described in Sect. 4.2. The difference in the determined metallicity of the components in the system was found to be 0.01 dex, which agrees with coeval star formation. We note, however, that the best-fit synthetic spectrum does not give a satisfactory fit for all atomic lines since the stronger lines tend to be too broad for the established fit. This affect can arise from an incorrect surface gravity, although the potassium line test described above does not support this explanation.

The third binary system, HD 101930 AB, consists of an early K-dwarf primary (K2) and an early M dwarf (M0-M1). The secondary is the only early M dwarf in our sample, and we note that the spectrum shows both features we recognise from the primary, such as strong Si lines, and characteristics seen in the other M dwarfs, such as absent C lines and prominent FeH lines. In a careful study of the best-fit synthetic spectrum, we noted that a majority of the lines fit rather well except for the strong Si lines and the excluded K lines. We derived a metallicity of 0.09 dex, which is 0.11 dex lower than established for the primary of the system. This difference is still consistent with the estimated uncertainties.

5.2. Single M dwarfs

For five of the eight single M dwarfs we derived metallicities for the first time based on high-resolution spectroscopy. For the three stars analysed in the optical by Bean et al. (2006a), our metallicities are higher by ≳0.2 dex. The recent study using spectroscopic indices by Rojas-Ayala et al. (2010) includes four of our targets, and we derived lower metallicities for three of these stars. The photometric calibration by Bonfils et al. (2005a) returns overall lower metallicities than we determined, but the calibration is claimed by Johnson & Apps (2009) to produce [Fe/H] values that are too low. These authors corrected for this, and we do agree better with this higher metallicity scale. We seem to find the best agreement with Schlaufman & Laughlin (2010), who used a similar technique to Johnson & Apps (2009). After the completion of the present paper, we noted that Neves et al. (2012) recently evaluated the photometric metallicity calibrations of Bo05, JA10 and SL10, and rank the SL10 scale highest. The metallicities derived in our work are shown in Figs. 5 and 6, together with results from the discussed studies. The average differences between our study and those of Schlaufman & Laughlin (2010), Johnson & Apps (2009), and Bonfils et al. (2005a) are 0.09, 0.13, and 0.17, respectively.

6. Conclusions

We have derived a new metallicity scale based on a careful spectroscopic analysis of high-resolution spectra ($R \sim 50\,000$) obtained in the J band. Previous abundance studies are based on full spectroscopic analyses in the optical regime, low-resolution spectroscopic infrared indices, as well as purely photometric calibrations. Observations in the infrared J band have the advantage of its few and weak molecular features (FeH), which allows for a precise continuum placement as compared to the optical wavelength regions where the continuum is heavily depressed due to the many and strong TiO lines. We find that we can correct for lines introduced by the Earth's atmosphere quite succesfully by using a rapidly rotating calibration star and by applying a carefully determined continuum placement. We verified the accuracy of the atmospheric models involved in the metallicity determination by observing three binary systems that are expected to have the same [Fe/H]. In two of the systems, GJ105 AB and GJ250 AB, we found that the metallicities agree within 0.01 and 0.02 dex, respectively. In the third binary system, HD 101930 AB, we found a discrepancy of 0.11 dex, which is consistent with the derived errors.

We tested the convergence of the procedure by starting from different initial guesses and found consistent solutions, although some of the cooler objects show a greater spread in the determined metallicity.

Our sample covers a restricted range in $T_{\rm eff}$ (between ≈3200 and 3400 K, and a single object at 3900 K), and the extreme metallicities (<−0.1 and >+0.2) are not well covered. To explore the metallicity scale further, targets with a wider spread in the

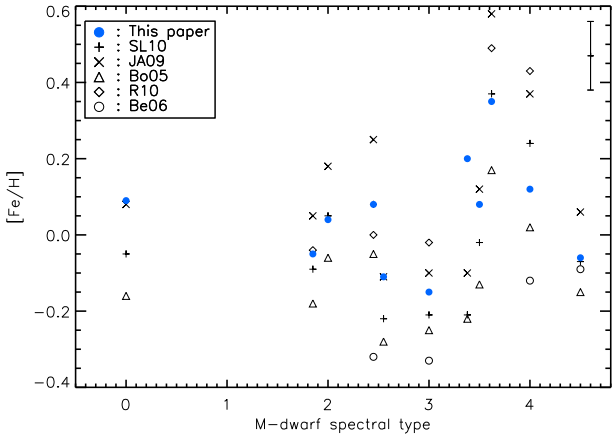

Fig. 5. Derived metallicities for our sample in comparison with previous abundance determinations (see Table 6 for references) as a function of spectral type (see Table 1). For an easier presentation the targets with equal spectral types have been slightly shifted horizontally. In the upper right corner we show an error bar indicating the mean error of the metallicities derived in this paper.

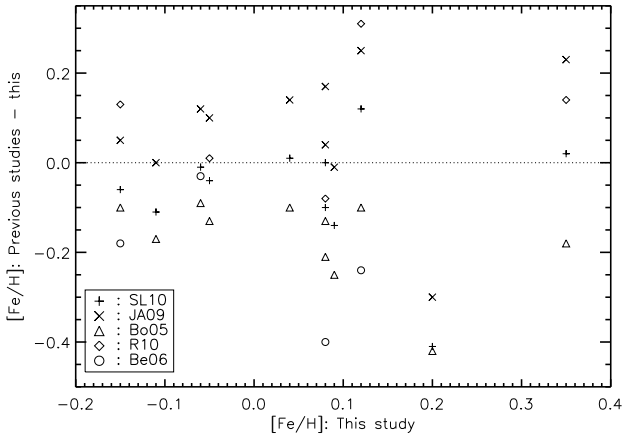

Fig. 6. Differences in metallicities for our sample in comparison with previous abundance determinations (see Table 6 for references) as a function of metallicities from this study. A zero-line (dotted) to guide the eye is also plotted.

atmospheric parameters need to be observed, preferably with an instrument that can cover a larger wavelength range efficiently. Improving the completeness of molecular line lists will improve the accuracy of the metallicity determinations, since there are still a number of unknown molecular blends present.

We conclude that high-resolution spectroscopic analysis in the near infrared is a reliable method for determining metallicities in this $T_{\rm eff}$ regime. It is also the only method that will enable the determination of abundances of individual elements in M dwarfs.

Acknowledgements. We thank Jeff Valenti for developing SME, and for providing additional IDL routines that were used in the analysis. UH acknowledges support from the Swedish National Space Board (Rymdstyrelsen). AÖ acknowledges support by Värmlands nation (Uddeholms research scholarship). This research has made use of the SIMBAD database, operated at the CDS, Strasbourg, France. NSO/Kitt Peak FTS data used here were produced by NSF/NOAO. This publication makes use of data products from the Two Micron All Sky Survey, which is a joint project of the University of Massachusetts and the Infrared Processing and Analysis Center/California Institute of Technology, funded by the National Aeronautics and Space Administration and the National Science Foundation.

References

Allard, F., & Hauschildt, P. H. 1995, ApJ, 445, 433
Allende Prieto, C., Barklem, P. S., Lambert, D. L., & Cunha, K. 2004, A&A, 420, 183
Asplund, M. 2005, ARA&A, 43, 481
Auman, Jr., J. R. 1969, ApJ, 157, 799
Barber, R. J., Tennyson, J., Harris, G. J., & Tolchenov, R. N. 2006, MNRAS, 368, 1087
Barklem, P. S., Piskunov, N., & O'Mara, B. J. 2000, A&AS, 142, 467 (BPM)
Bean, J. L., Benedict, G. F., & Endl, M. 2006a, ApJ, 653, L65
Bean, J. L., Sneden, C., Hauschildt, P. H., Johns-Krull, C. M., & Benedict, G. F. 2006b, ApJ, 652, 1604
Bessel, M. S. 1990, A&AS, 83, 357
Biémont, E., & Brault, J. W. 1986, Phys. Scr., 34, 751
Blackwell-Whitehead, R. J., Lundberg, H., Nave, G., et al. 2006, MNRAS, 373, 1603 (BLNP)
Bonfils, X., Delfosse, X., Udry, S., et al. 2005a, A&A, 442, 635
Bonfils, X., Forveille, T., Delfosse, X., et al. 2005b, A&A, 443, L15
Bonfils, X., Mayor, M., Delfosse, X., et al. 2007, A&A, 474, 293
Brett, J. M. 1995a, A&A, 295, 736
Brett, J. M. 1995b, A&AS, 109, 263
Brett, J. M., & Plez, B. 1993, PASA, 10, 250
Browning, M. K., Basri, G., Marcy, G. W., West, A. A., & Zhang, J. 2010, AJ, 139, 504
Burrows, A., Ram, R. S., Bernath, P., Sharp, C. M., & Milsom, J. A. 2002, ApJ, 577, 986
Butler, R. P., Vogt, S. S., Marcy, G. W., et al. 2004, ApJ, 617, 580
Butler, R. P., Johnson, J. A., Marcy, G. W., et al. 2006, PASP, 118, 1685
Carpenter, J. M. 2001, AJ, 121, 2851
Casagrande, L., Flynn, C., & Bessell, M. 2008, MNRAS, 389, 585
Chabrier, G. 2003, PASP, 115, 763
Chang, T. N., & Tang, X. 1990, J. Quant. Spectrosc. Radiat. Transf., 43, 207
Cousins, A. W. J. 1980, South African Astron. Observ. Circ., 1, 166
Cousins, A. W. J., & Stoy, R. H. 1962, Roy. Greenwich Obs. Bull., 64, 103
Cutri, R. M., Skrutskie, M. F., van Dyk, S., et al. 2003, 2MASS All Sky Catalog of point sources
Delfosse, X., Forveille, T., Perrier, C., & Mayor, M. 1998, A&A, 331, 581
Delfosse, X., Forveille, T., Ségransan, D., et al. 2000, A&A, 364, 217
Dommanget, J., & Nys, O. 2002, VizieR Online Data Catalog, 1274, 0
Dubernet, M. L., Boudon, V., Culhane, J. L., et al. 2010, J. Quant. Spec. Radiat. Transf., 111, 2151
Dulick, M., Bauschlicher, Jr., C. W., Burrows, A., et al. 2003, ApJ, 594, 651
Endl, M., Cochran, W. D., Wittenmyer, R. A., & Boss, A. P. 2008, ApJ, 673, 1165
Fischer, D. A., & Valenti, J. 2005, ApJ, 622, 1102
Golimowski, D. A., Fastie, W. G., Schroeder, D. J., & Uomoto, A. 1995a, ApJ, 452, L125
Golimowski, D. A., Nakajima, T., Kulkarni, S. R., & Oppenheimer, B. R. 1995b, ApJ, 444, L101
Gray, R. O., Corbally, C. J., Garrison, R. F., et al. 2006, AJ, 132, 161
Grevesse, N., Asplund, M., & Sauval, A. J. 2007, Space Sci. Rev., 130, 105
Gustafsson, B., Edvardsson, B., Eriksson, K., et al. 2008, A&A, 486, 951
Hauschildt, P. H., Allard, F., & Baron, E. 1999, ApJ, 512, 377
Hawley, S. L., Gizis, J. E., & Reid, I. N. 1996, AJ, 112, 2799
Heiter, U., & Luck, R. E. 2003, AJ, 126, 2015
Henry, T. J. 1998, in Brown Dwarfs and Extrasolar Planets, ed. R. Rebolo, E. L. Martin, & M. R. Zapatero Osorio, ASP Conf. Ser., 134, 28
Hibbert, A., Biémont, E., Godefroid, M., & Vaeck, N. 1993, A&AS, 99, 179
Holmberg, J., Nordström, B., & Andersen, J. 2009, A&A, 501, 941
Jenkins, J. S., Ramsey, L. W., Jones, H. R. A., et al. 2009, ApJ, 704, 975
Johnson, J. A., & Apps, K. 2009, ApJ, 699, 933
Johnson, J. A., Butler, R. P., Marcy, G. W., et al. 2007, ApJ, 670, 833
Jones, H. R. A., & Tsuji, T. 1997, ApJ, 480, L39
Kaeufl, H.-U., Ballester, P., Biereichel, P., et al. 2004, in SPIE Conf. Ser. 5492, ed. A. F. M. Moorwood, & M. Iye, 1218
Kharchenko, N. V. 2001, Kinematika i Fizika Nebesnykh Tel, 17, 409
Kilkenny, D., van Wyk, F., Roberts, G., Marang, F., & Cooper, D. 1998, MNRAS, 294, 93
Kilkenny, D., Koen, C., van Wyk, F., Marang, F., & Cooper, D. 2007, MNRAS, 380, 1261
Koen, C., Kilkenny, D., van Wyk, F., Cooper, D., & Marang, F. 2002, MNRAS, 334, 20
Koen, C., Kilkenny, D., van Wyk, F., & Marang, F. 2010, MNRAS, 403, 1949
Kupka, F., Piskunov, N., Ryabchikova, T. A., Stempels, H. C., & Weiss, W. W. 1999, A&AS, 138, 119
Kurucz, R. 1994a, Atomic Data for Ca, Sc, Ti, V, and Cr, Kurucz CD-ROM No. 20, Cambridge, Mass.: Smithsonian Astrophysical Observatory, 20

Kurucz, R. 1994b, Atomic Data for Mn and Co. Kurucz CD-ROM No. 21, Cambridge, Mass.: Smithsonian Astrophysical Observatory, 21
Kurucz, R. L. 2007, On-line database of observed and predicted atomic transitions, http://kurucz.harvard.edu/atoms/1400/, http://kurucz.harvard.edu/atoms/2000/, http://kurucz.harvard.edu/atoms/2500/, http://kurucz.harvard.edu/atoms/2600/
Kurucz, R. L. 2010, On-line database of observed and predicted atomic transitions, http://kurucz.harvard.edu/atoms/2200, http://kurucz.harvard.edu/atoms/2400
Laing, J. D. 1989, South African Astron. Observ. Circ., 13, 29
Langhoff, S. R., & Bauschlicher, C. W. 1990, J. Mol. Spectrosc., 141, 243
Livingston, W., & Wallace, L. 1991, An atlas of the solar spectrum in the infrared from 1850 to 9000 cm^{-1} (1.1 to 5.4 micrometer)
Lovis, C., Mayor, M., Bouchy, F., et al. 2005, A&A, 437, 1121
Luck, R. E., & Heiter, U. 2006, AJ, 131, 3069
Marcy, G. W., Butler, R. P., Vogt, S. S., Fischer, D., & Lissauer, J. J. 1998, ApJ, 505, L147
Marcy, G. W., & Chen, G. H. 1992, ApJ, 390, 550
McLean, I. S., Wilcox, M. K., Becklin, E. E., et al. 2000, ApJ, 533, L45
McLean, I. S., Prato, L., McGovern, M. R., et al. 2007, ApJ, 658, 1217
Meléndez, J., & Barbuy, B. 1999, ApJS, 124, 527
Mishenina, T. V., Soubiran, C., Kovtyukh, V. V., & Korotin, S. A. 2004, A&A, 418, 551
Mould, J. R. 1975, A&A, 38, 283
Mould, J. R. 1976, A&A, 48, 443
Mugrauer, M., Neuhäuser, R., Mazeh, T., Alves, J., & Guenther, E. 2004, A&A, 425, 249
Mugrauer, M., Neuhäuser, R., Seifahrt, A., Mazeh, T., & Guenther, E. 2005, A&A, 440, 1051
Mugrauer, M., Seifahrt, A., & Neuhäuser, R. 2007, MNRAS, 378, 1328
Neves, V., Bonfils, X., Santos, N. C., et al. 2012, A&A, 538, A25
Nussbaumer, H., & Storey, P. J. 1984, A&A, 140, 383
O'Brian, T. R., Wickliffe, M. E., Lawler, J. E., Whaling, W., & Brault, J. W. 1991, J. Opt. Soc. Am. B Opt. Phys., 8, 1185 (BWL)
Phillips, J. G., Davis, S. P., Lindgren, B., & Balfour, W. J. 1987, ApJS, 65, 721
Poveda, A., Herrera, M. A., Allen, C., Cordero, G., & Lavalley, C. 1994, Rev. Mex. Astron. Astrofis., 28, 43
Ralchenko, Y., Kramida, A., Reader, J., & NIST ASD Team. 2010, NIST Atomic Spectra Database (ver. 4.0.0), http://physics.nist.gov/asd
Reid, I. N., Hawley, S. L., & Gizis, J. E. 1995, AJ, 110, 1838
Reid, I. N., Cruz, K. L., Allen, P., et al. 2004, AJ, 128, 463
Reiners, A. 2007, A&A, 467, 259
Rojas-Ayala, B., Covey, K. R., Muirhead, P. S., & Lloyd, J. P. 2010, ApJ, 720, L113
Salpeter, E. E. 1955, ApJ, 121, 161
Santos, N. C., Israelian, G., & Mayor, M. 2004, A&A, 415, 1153
Santos, N. C., Israelian, G., Mayor, M., et al. 2005, A&A, 437, 1127
Schlaufman, K. C., & Laughlin, G. 2010, A&A, 519, A105
Schneider, J., Dedieu, C., Le Sidaner, P., Savalle, R., & Zolotukhin, I. 2011, A&A, 532, A79
Shulyak, D., Seifahrt, A., Reiners, A., Kochukhov, O., & Piskunov, N. 2011, MNRAS, 418, 2548
Sousa, S. G., Santos, N. C., Mayor, M., et al. 2008, A&A, 487, 373
The, P. S., Steenman, H. C., & Alcaino, G. 1984, A&A, 132, 385
Torres, C. A. O., Quast, G. R., da Silva, L., et al. 2006, A&A, 460, 695
Tsuji, T. 1969, in Low-Luminosity Stars, ed. S. S. Kumar, 457
Tsuji, T. 2002, ApJ, 575, 264
Upgren, A. R., Grossenbacher, R., Penhallow, W. S., MacConnell, D. J., & Frye, R. L. 1972, AJ, 77, 486
Valenti, J. A., & Fischer, D. A. 2005, ApJS, 159, 141
Valenti, J. A., & Piskunov, N. 1996, A&AS, 118, 595
van Leeuwen, F., ed. 2007, Hipparcos, the New Reduction of the Raw Data, Astrophys. Space Sci. Libr., 350
van Maanen, A. 1938, ApJ, 88, 27
Vieira, T. 1986, Ph.D. Thesis, Uppsala Astronomical Observatory, Uppsala University
Wende, S., Reiners, A., & Ludwig, H.-G. 2009, A&A, 508, 1429
Wende, S., Reiners, A., Seifahrt, A., & Bernath, P. F. 2010, A&A, 523, A58
Woolf, V. M., & Wallerstein, G. 2005, MNRAS, 356, 963
Woolf, V. M., & Wallerstein, G. 2006, PASP, 118, 218
Worthey, G., & Lee, H.-C. 2011, ApJS, 193, 1
Zhang, H. W., Butler, K., Gehren, T., Shi, J. R., & Zhao, G. 2006, A&A, 453, 723

Table 2. Atomic lines used in the analysis.

Wavelength [Å]	Species	E_{low} [eV]	log gf	VdW	Source	K/M
11 681.594	Fe I	3.547	−3.301	−7.352	S(4)	K
11 682.250	Fe I	5.620	−1.420	−7.520	7	K
11 715.487	Fe I	5.642	−0.961	−7.142	S(4)	K
11 725.563	Fe I	5.699	−1.279	−7.11 2	S(4)	K
11 727.733	Fe I	6.325	−0.879	−6.722	S(4)	K
11 743.695	Fe I	5.947	−0.943	−6.932	S(4)	K (P82)
11 767.600	Ca I	4.532	−0.635	−6.777	S(4)	K, M
11 780.547	Ti I	1.443	−2.180	−7.790	2, 3	K, M
11 783.267	Fe I	2.832	−1.520	−7.842	S(8, 4)	K, M
11 783.433	Mn I	5.133	−0.094	−7.560	4	K
11 797.179	Ti I	1.430	−2.250	−7.790	2, 3	K, M
11 828.171	Mg I	4.346	−0.046	862.225	S(9), 1	K, M (P82)
11 949.545	Ti I	1.443	−1.550	−7.790	2, 3	K, M
11 949.760	Ca II	6.470	−0.040		7	K
11 955.955	Ca I	4.131	−0.849	−7.300	4	K, M
11 973.050	Fe I	2.176	−1.405	−7.889	S(8, 4)	K, M
11 973.854	Ti I	1.460	−1.591	−7.528	S(2, 3)	K, M
11 984.198	Si I	4.930	+0.239	677.228	4, 1	K
11 991.568	Si I	4.920	−0.109	674.228	4, 1	K
12 031.504	Si I	4.954	+0.477	685.229	4, 1	K
12 039.822	Mg I	5.753	−1.530		9	K
12 044.055	Cr I	3.422	−1.863	−6.281	3	K
12 044.129	Fe I	4.988	−2.130	−6.677	4	K
12 053.083	Fe I	4.559	−1.543	−7.540	8, 4	K
12 510.520	Fe I	4.956	−1.846	−7.142	S(4)	K
12 532.835	Cr I	2.709	−1.879	−7.800	3	K, M
12 556.999	Fe I	2.279	−3.913	−7.422	S(8, 4)	K, M
12 569.569	Ti I	2.175	−1.867	−7.810	5	K, M
12 569.634	Co I	3.409	−0.992	−7.730	6	K
12 600.277	Ti I	1.443	−2.150	−7.790	2, 3	K, M
12 909.070	Ca I	4.430	−0.426	−7.787	5	M (P84)
12 910.087	Cr I	2.708	−1.863	−7.402	S(3)	M (P84)
12 919.898	Ti I	2.154	−1.553	−7.750	3	M (P84)
12 937.016	Cr I	2.710	−1.896	−7.800	3	M (P84)
12 975.927	Mn I	2.888	−1.356	−7.372	S(4)	M (P84)
12 975.72–12 976.15[a]	Mn I				S(7)	M (P84)
13 001.401	Ca I	4.441	−1.139	−7.710	4	M (P84)
13 006.685	Fe I	2.990	−3.269	−7.412	S(4)	M (P84)
13 011.892	Ti I	1.443	−2.180	−7.790	2, 3	M (P84)
13 033.555	Ca I	4.441	−0.064	−7.710	4	M (P84)
13 057.885	Ca I	4.441	−1.092	−7.710	4	M (P84)

Notes. Column descriptions: E_{low}: lower level energy. "VdW": parameter(s) used to calculate line broadening due to van der Waals interaction; negative numbers: logarithm of the line width per perturber at 10^4 K in rad s^{-1} cm^3 (log γ_W); positive numbers: integer part: broadening cross-section at a velocity of 10^4 m s^{-1} in atomic units, fractional part: velocity parameter (see Barklem et al. 2000). "Source": reference code for the atomic data (see below), or "S": log gf and log γ_W determined from a fit to the solar spectrum (reference code in parentheses: source of the initial data); if two codes: log gf, log γ_W. "K/M": line was used in K- or M-dwarf analysis (some only in the P82 or P84 spectra, see Table 1). [(a)] Blend of eight Mn I lines.

References. 1) Barklem et al. (2000); 2) Blackwell-Whitehead et al. (2006); 3) Kurucz (2010); 4) Kurucz (2007); 5) Kurucz (1994a); 6) Kurucz (1994b); 7) Meléndez & Barbuy (1999); 8) O'Brian et al. (1991); 9) Ralchenko et al. (2010); Biémont & Brault (1986); Chang & Tang (1990).